Mechanics of Materials 43 (2011) 313–331

Contents lists available at ScienceDirect

Mechanics of Materials

journal homepage: www.elsevier.com/locate/mechmat

A dual conical indentation technique based on FEA solutions for property evaluation

Hong Chul Hyun [a,*], Minsoo Kim [a], Jin Haeng Lee [b], Hyungyil Lee [a]

[a] Sogang University, Department of Mechanical Engineering, Seoul 121-742, Republic of Korea
[b] Division for Research Reactor, Korea Atomic Energy Research Institute, Daejeon 305-353, Republic of Korea

ARTICLE INFO

Article history:
Received 24 February 2010
Received in revised form 17 February 2011
Available online 3 April 2011

Keywords:
Conical indenter
Dual-conical indentation
Material property
Contact diameter
Tip-radius
Reverse analysis

ABSTRACT

The sharp indenters such as Berkovich and conical indenters have a geometrical self-similarity so that we can obtain only one parameter from an indentation loading curve, which makes different materials have the same load–displacement relation. Most studies to evaluate elastic–plastic properties by using the geometrical self-similar indenter have therefore tried to use dual/plural indentation techniques, on the basis of the concept of representative strain/stress varying with the indenter angle. However, any suggested representative concept is not universally operative for real materials. In this work, we suggest a method of material property evaluation without using the concept of representative strain. We begin the work by studying the characteristics of load–depth curves of conical indenters via finite element (FE) method. From FE analyses of dual-conical indentation, we investigate the relationships between indentation parameters and load–depth curves. The projected contact diameter is expressed as a function of the indenter angle, tip-radius, and material properties, which allows us to simply predict the elastic modulus. Two mapping functions for two indenter angles (45° and 70.3°) are presented to find the two unknowns (yield strain and strain-hardening exponent) via dual indentation technique. The method provides elastic modulus, yield strength and strain-hardening exponent with an average error of less than 5%. The method is valid for any elastically deforming indenters. We also discuss the sensitivity of measured properties to the load–displacement curve variation, and the difference between conical and Berkovich indenters.

1. Introduction

The instrumented indentation test is a method to extract material properties from indentation load–depth curves with micro specimens or parts of mechanical structures in use (Chen et al., 2006, 2010; Cook and Pharr, 1990; Giannakopoulos and Larsson, 1997; Giannakopoulos and Suresh, 1999; Huber and Tsakmakis, 1999a,b; Kermouche et al., 2008; Lan and Venkatesh, 2007; Lee et al., 2005; Liao et al., 2009; Ogasawara et al., 2006a,b, 2009; Oliver and Pharr, 1992; Suresh and Giannakopoulos, 1998; Xia et al., 2007). The contact area and load–displacement curves to measure the hardness and elastic modulus are fundamental and important data for indentation test. However, it is quite difficult to measure or predict the contact diameter due to imperfection or tip-blunting of indenter. Based on Hertz contact mechanics, many studies on evaluating the actual contact area and geometric deviation of indenter from its nominal geometry have been performed (Borodich et al., 2003; Borodich and Keer, 2004).

There should be a one-to-one match between the load–depth curve obtained from an indentation test and its material properties. However, some materials having different material properties may show the same load–depth curve due to the geometrical self-similarity of sharp indenters (Capehart and Cheng, 2003; Chen et al., 2007; Cheng and Cheng, 1998; Lee et al., 2008; Tho et al., 2004). Chen

* Corresponding author. Tel.: +82 2 705 8636; fax: +82 2 712 0799.
E-mail address: hchyun@sogang.ac.kr (H.C. Hyun).

0167-6636/$ - see front matter © 2011 Elsevier Ltd. All rights reserved.
doi:10.1016/j.mechmat.2011.03.003

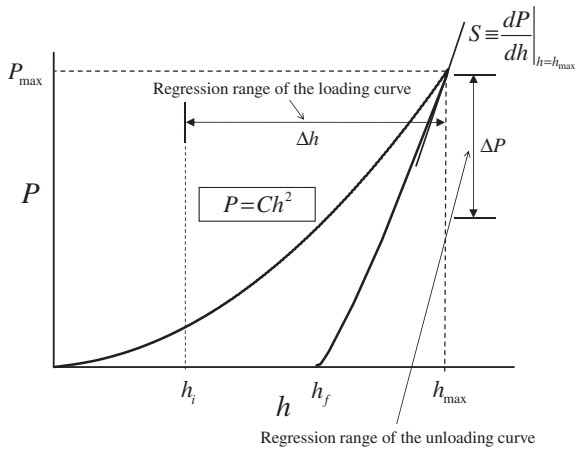

Fig. 1. Schematic illustration of a *P*–*h* curve of elastic–plastic material under instrumented sharp indentation (Lee et al., 2008).

et al. (2007) and Lee et al. (2008) demonstrated that countless materials can have the same Kick's law coefficient *C* despite their different material properties. Dual (plural) sharp indenters with dissimilar angles can be therefore used to solve this problem. In previous studies (Bucaille et al., 2003; Cao and Lu, 2004; Chollacoop et al., 2003; Ogasawara et al., 2005, 2006a; Shim et al., 2008), unique solutions were attempted by using the concept of representative strain ε_R which varies with the half-included angle of indenter.

The loading curves from sharp indenters generally follow the Kick's law relation.

$$P = Ch^2 \tag{1}$$

Here P is the indentation load, h is the measured depth from reference surface and C is the coefficient of the Kick's law. P_{max} is the maximum load at the maximum indentation depth h_{max}, and the initial unloading slope S is defined as dP/dh at $h = h_{max}$ as depicted in Fig. 1. Kick's law is valid for the ideal sharp indenter, but the tip-radius effect breaks the Kick's law and the corresponding self-similarity. For eliminating the effect of tip-radius, Lee et al. (2008) suggested the corrected Kick's law as following equation.

$$P = C(h + h_g)^2, \quad h_g = R\left(\frac{1}{\sin\alpha} - 1\right) \tag{2}$$

Here h_g is the gap between the indenters with zero and finite tip-radius (Fig. 2). Eq. (2) is not valid when the effect of the tip-radius is dominant in shallow indentation. However, as the indentation depth increases the effect of the tip-radius decreases so Eq. (2) became valid. In Fig. 2, h_t means the expected indentation depth ($h_t = h + h_g$) for an ideally sharp indenter.

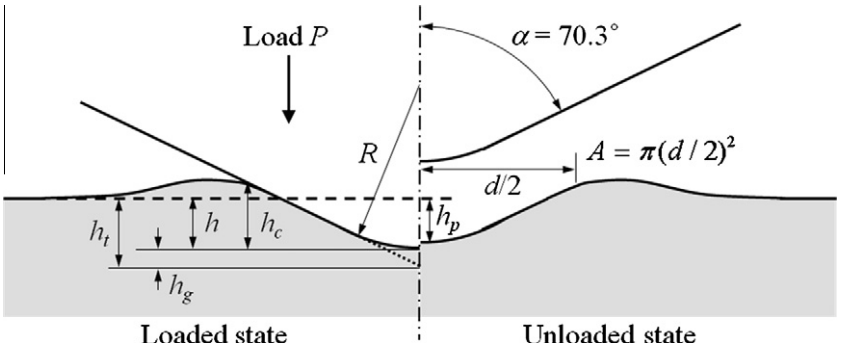

Fig. 2. Schematic of sharp indentation profiles with finite tip-radius.

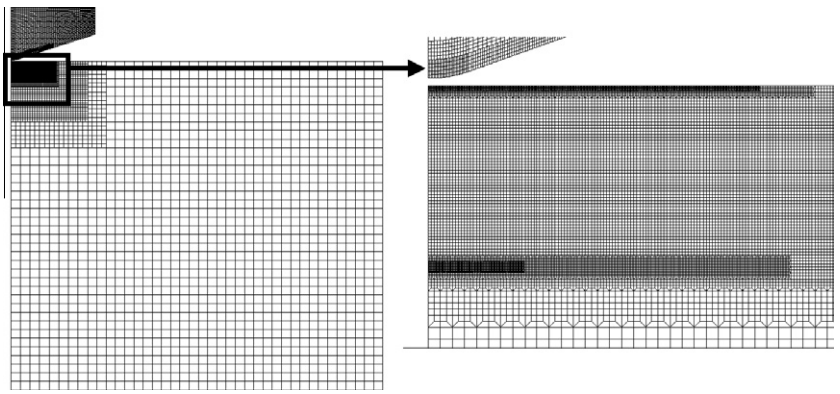

Fig. 3. Overall mesh design using axisymmetric conical indenter.

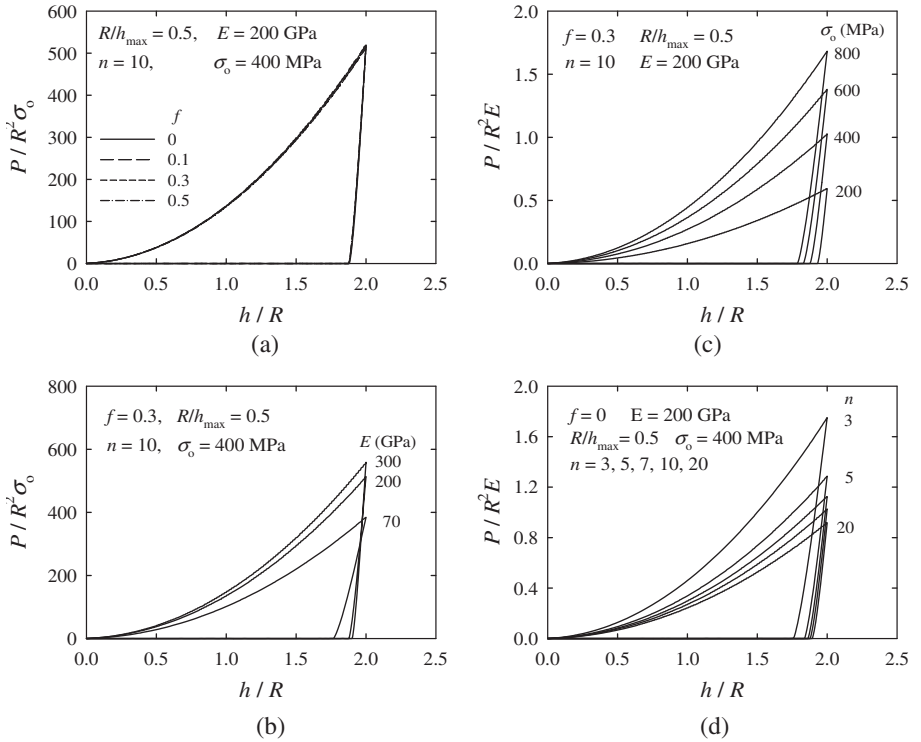

Fig. 4. Load–depth curves for various values of indentation parameters.

P/h^2 is a constant value independent of indentation depth, so the representative strain which shows the deformation state of materials has a unique value. In most previous studies, the main objective is to determine the way of defining the representative strain and its value. They tried to reduce the number of indentation parameters using the representative strain. The concept of the representative strain was introduced by Tabor (1951) ($\varepsilon_R = 0.08$ for Vickers indentation). Dao et al. (2001) ($\varepsilon_R = 0.033$) found out that stress–strain curves of materials having the same Kick's law coefficient C exhibit the same true stress at the plastic strain of 3.3% for 70.3° conical indentation. Dao et al. (2001) presented then the following dimensionless function.

$$\Pi\left(\frac{E_e}{\sigma_R}, n\right) = \frac{C}{\sigma_R} \tag{3}$$

Here σ_R is the representative stress corresponding to ε_R, n is the strain-hardening exponent, and E_e is the effective modulus. Dao et al. (2001) used the following relation between representative stress and representative strain.

$$\sigma_R = \sigma_o\left(1 + \frac{E}{\sigma_o}\varepsilon_R\right)^n \tag{4}$$

Here σ_o is the yield strength and E is the elastic modulus. The concepts of dual conical indentation were suggested by Bucaille et al. (2003) ($\varepsilon_R = 0.105 \cot \alpha$) and Chollacoop et al. (2003) ($\varepsilon_R = -2.185 \times 10^{-3}\alpha + 0.1894$). Here α is the half-included angle of a conical indenter (Fig. 2). They ob-

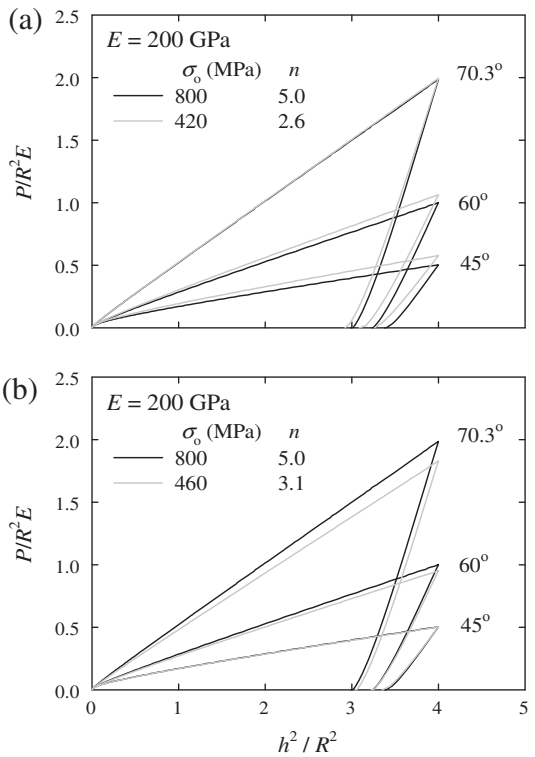

Fig. 5. P/P_{max} vs. h^2 curves for different material properties with the same C and E for (a) $\alpha = 70.3°$ and (b) $\alpha = 45°$.

Table 1
Comparison of C values with three half-included angles.

α (°)	Kick's law coefficient C (GPa)					
	σ_o = 800 MPa n = 5.0	σ_o = 420 MPa n = 2.6	Gap (%)	σ_o = 800 MPa n = 5.0	σ_o = 600 MPa n = 3.7	Gap (%)
45.0	17.6	20.2	14.9	17.6	17.5	0.3
60.0	43.9	46.7	6.4	43.9	41.7	4.5
70.3	96.5	97.0	0.6	96.5	88.7	8.1

Table 2
Material properties for FE analyses.

Material property of indenters	Material property	Values used in FEA
WC (E_I = 537 GPa, ν_I = 0.24)	Young's modulus (GPa)	70, 200, 300
	Poisson's ratio	0.3
	Yield strength (MPa)	200, 400, 600, 800, 1200, 1600, 2000
	Strain-hardening exponent	1.1, 2, 3, 5, 7, 10, 13, 20

tained multiple equations by substituting ε_R and σ_R values of two indenter angles into Eq. (4), and then determined σ_o and n. Thereafter, Cao and Lu (2004) suggested some conditions which should be satisfied to use the above method. Ogasawara et al. (2005) (ε_R = 0.0139 cot α for 70.3° conical indentation defined the representative strain as a function of plastic strain related to axisymmetric deformation. Their representative stress corresponding to the representative strain is determined by the following Eq. (5).

$$\sigma_R = R\left(2\frac{\sigma_R}{E} + 2\varepsilon_R\right)^n \tag{5}$$

Chen et al. (2007) and Ogasawara et al. (2006) noted that C/σ_R varies linearly with respect to E_e/σ_R when its value is very small (elastic limit), and C/σ_R asymptotically approaches to a constant value as E_e/σ_R increases (rigid plastic limit). They suggested the function C/σ_R using the elastic limit and the rigid plastic limit.

$$\Pi = \frac{C}{\sigma_R} = \left(\frac{1}{m_e \frac{E_e}{\sigma_R}} + \frac{1}{m_p}\right)^{-1} \tag{6}$$

Here m_e is the slope of the linear region, m_p is the rigid plastic limit. However, some materials having different properties still show almost the same C in dual (or plural) indentation, so Chen et al. (2007) named them "mystical materials". As the difference of the angles, $\Delta\alpha$, gets bigger, the region of "mystical materials" decreases. However, Chen et al. (2007) have shown neither a systematic way

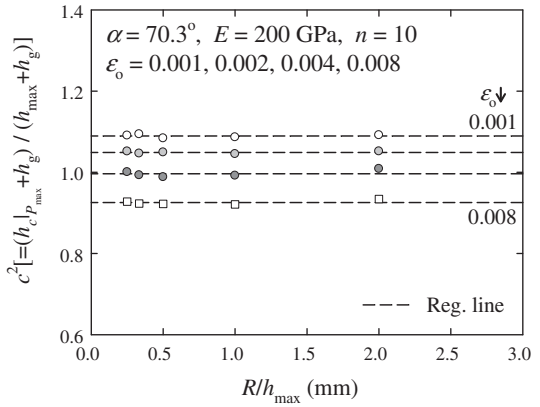

Fig. 6. c^2 vs. indentation depths for four different yield strains.

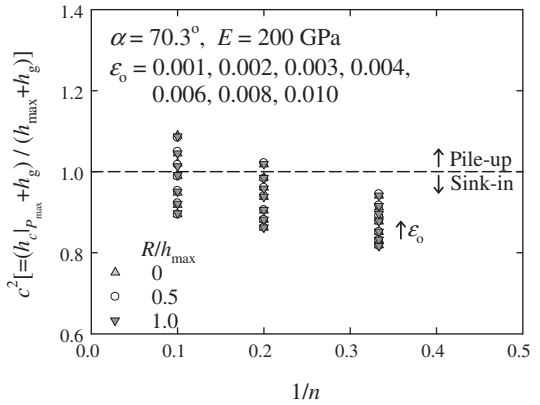

Fig. 7. c^2 vs. $1/n$ for three different various tip radii.

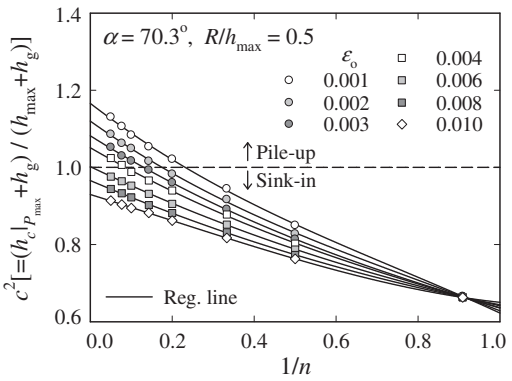

Fig. 8. c^2 vs. $1/n$ curves for various values of yield strain.

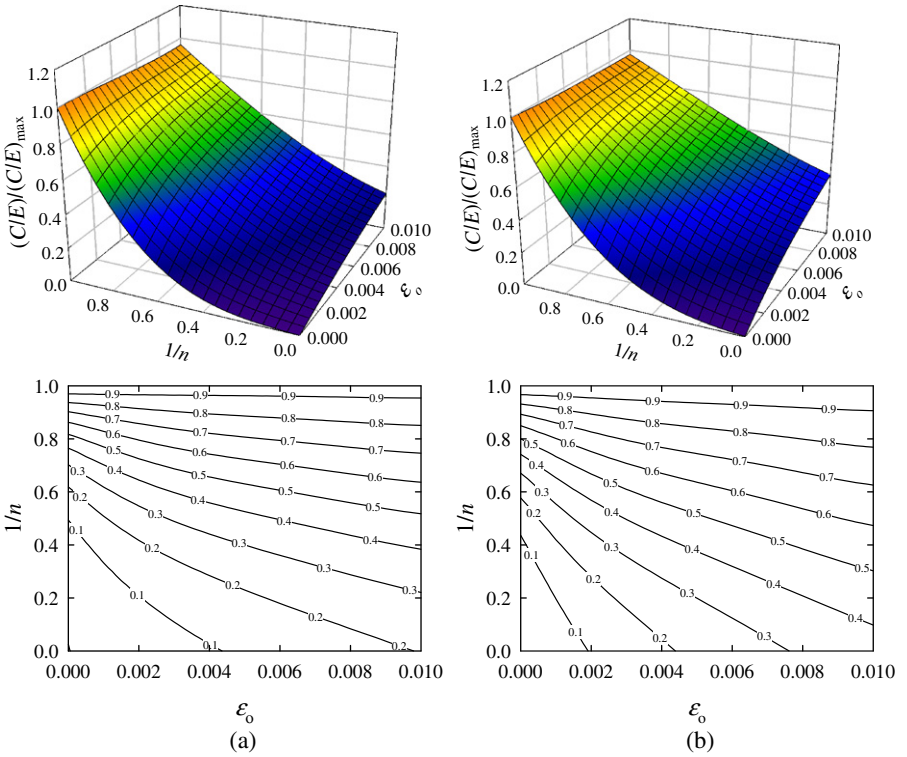

Fig. 9. 3D distribution of C/E & contour lines (a) $\alpha = 45°$, (b) $\alpha = 70.3°$.

of distinction nor an application to the non-power law materials.

As was stated above, the definitions and the variations of the representative strain with indenter angles were different in each previous study. In addition, suggested definitions of ε_R are disputable in their representativeness (Lee et al., 2010). We can imagine that two true stress–strain curves could be almost the same until the strain is less than ε_R but be different out of the region. If the representative strain is a function of indenter angle only, though

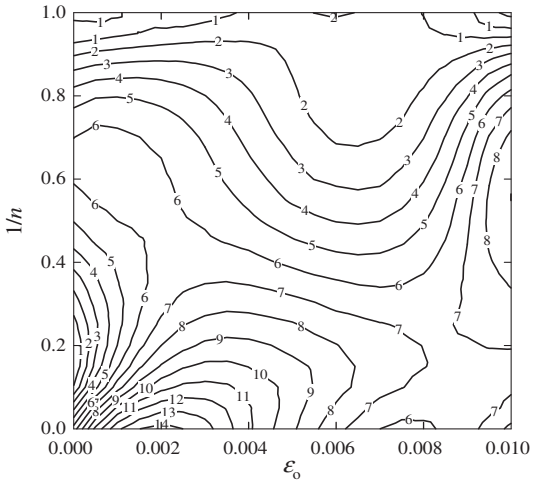

Fig. 10. Deference of angles between gradients of each contour line.

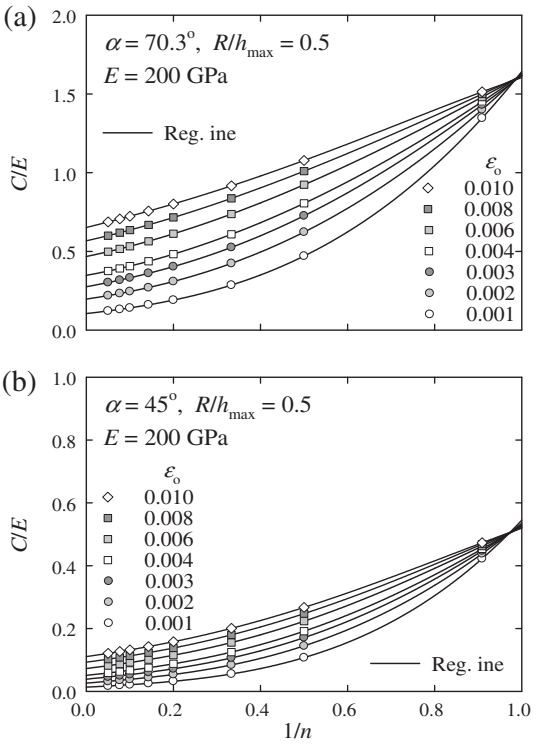

Fig. 11. C/E vs. $1/n$ curves for various values of yield strain.

material properties are different, two materials must have the same ε_R and σ_R. If the representative strain is smaller than about 0.3, the load–depth curves of two materials are different. This means that two materials which show the different load–depth curves have same ε_R and σ_R. Therefore, the representative strain must have a large value. Chaudhri (1998) and Giannakopoulos and Suresh (1999) suggested the ε_R = 0.25–0.36, but these values are too large to present the strain field of subindenter. To be representative, ε_R and σ_R should therefore vary with the material properties, and be a unique value for each material.

Swaddiwudhipong et al. (2005) and Le (2008, 2009) found the relationship between the characteristics of the load–displacement curves and the properties of elastic–plastic materials. Then, they built a reverse analysis algorithm for dual indentation. They predicted material properties using the change of various indentation variables such as C, unloading slope, and loading–unloading energies. Swaddiwudhipong et al. (2005) used the ratio of E_e/σ_o and n as two key parameters. However, the effective Young's modulus E_e cannot express the real material property, and the ratio of the Young's modulus to yield strength E/σ_o is more important than the ratio of the effective modulus to yield strength E_e/σ_o, based on our analysis. In addition, the maximum variation of predicted yield strength with experimental scatter for the loading curve is about 70%.

Like these, prior indentation theories have inherent restrictions on measurement of practical material properties. Even though FE analysis was used in some works, limited range of material property was considered and inappropriate methods were used as mentioned above. Only with verification for a wider range of real materials, the previous methods could be practical and reliable.

In this work, we suggest a method of material property evaluation by using a reverse analysis, which does not adopt the concept of representative strain. In the spherical indentation, it is difficult to evaluate the material properties without the defining a representative strain. In contrast, when geometrically self-similar indenters are used, the multiple indentations can be used to obtain the equations as many as the unknown values and it does not require defining the representative strain value. To establish the equations, we investigate the aspect of material deformations (pile-up/sink-in) near the contact area. If the measured (or calculated) contact area is inaccurate, large errors in predicting the elastic modulus or hardness may accompany. We also examine the contact mechanics of indenter with tip radius. In engineering practice, the indenter is not perfectly sharp but has a tip radius. Therefore, in shallow indentation there is only spherical contact; the material deformation in deep indentation obeys the conical contact mechanics. In this work, we analyzed the variation of contact radius and load–displacement curves with indenter tip radius. Based on the method proposed by Lee et al. (2008), we removed the effect of tip radius. Moreover, we investigate the variation of load–displacement curve with indent angle.

The paper is organized as follows. Section 2 shows the FE model (ABAQUS, 2007) and conditions for conical indentation. We observe the effect of material properties, friction coefficient and conical indenter's angle on the load–depth curves in Section 3. Section 4 presents the regression functions using the correlation among yield strains, strain hardening exponents and indentation load–depth curves. In addition, we provide the calculation method for contact diameter using regression function of material properties. We then propose a dual-conical indentation technique and verify the method. We also discuss the sensitivity of measured properties on the load–depth curve in Section 5. Finally, Section 6 shows the difference between conical and Berkovich indenters.

2. Finite element analysis

Fig. 3 shows the 2D FE model of the numerical conical indentation test that has the same projected contact area as the Berkovich indenter for the same indentation depth. We perform the finite element (FE) analyses using ABAQUS. We make an axisymmetric model considering that both load and configuration are axisymmetric. We carry out nonlinear geometry analyses using isotropic elastic–plastic material, which obeys J_2 flow theory.

We use the four-node axisymmetric element CAX4 (ABAQUS, 2007). We performed finite element analyses while changing the size of minimum element e, according to the indenter tip-radius R. It turned out that when R/e > 120, the element size effect is negligible, so we choose R/e = 160 as the minimum element size. Multi-Point Constraints (MPC) is conveniently used at the transition region where element size changes, but constrained mid-nodes of MPC tend to give discrete stress–strain values. We thus adopt trapezoidal elements in the transition region near the contact surface, and use MPC in only the transition region far from the contact surface. FE model consists of about 24900 4-node axisymmetric elements (CAX4) and 25400 nodes. We place contact surfaces at both material and indenter surfaces. Axisymmetric boundary conditions are imposed on the nodes on the axisymmetric axis. The indenter moves down to penetrate the material the bottom of which is fixed.

The Young's modulus and Poisson's ratio of WC indenter are taken by an ultrasonic test, which values are 537 GPa

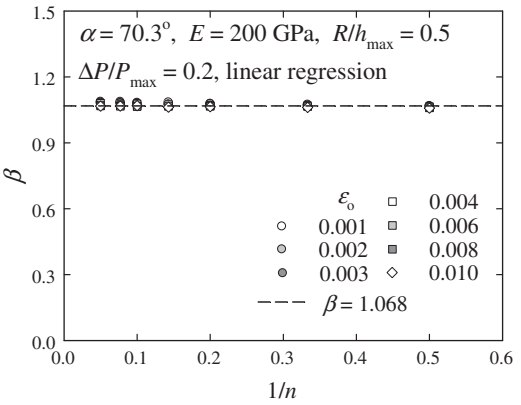

Fig. 12. β vs. $1/n$ curves for various values of yield strain.

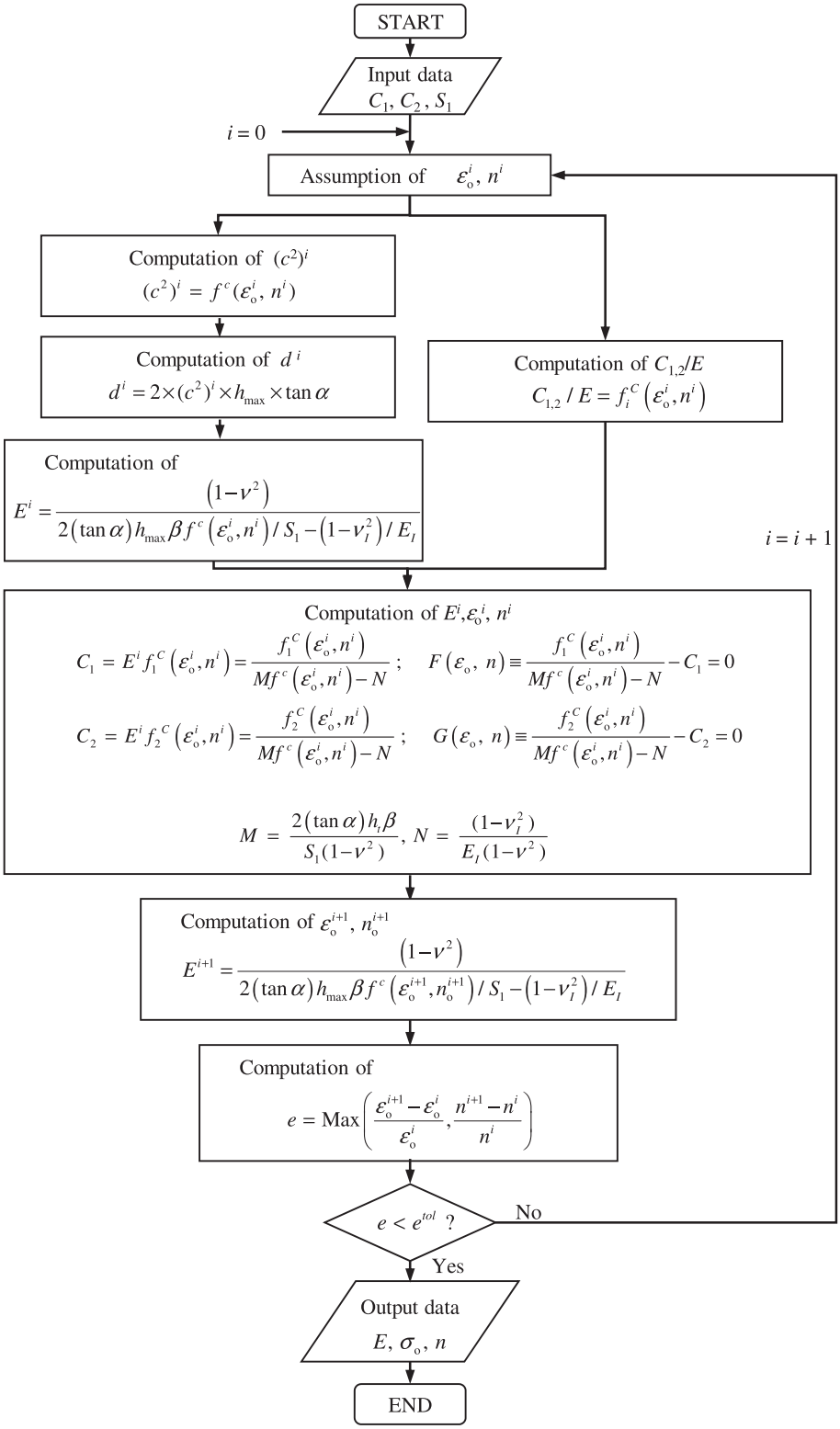

Fig. 13. Flow chart for determination of material properties.

and 0.24, respectively. To confirm the effect of the tip-radii, we vary the ratio of the tip-radius to the maximum indentation depth R/h_{max} between 0.5 and 2. Indentation formulas that developed WC indenter are valid even when Young's modulus and Poisson's ratio of WC indenter are substituted with those of diamond (Lee et al., 2008).

We need a regression equation for stress–strain curve and related material properties. The stress–strain curve can be expressed with piecewise power relationship (Rice and Rosengren, 1968).

$$\frac{\varepsilon_t}{\varepsilon_o} = \begin{cases} \frac{\sigma}{\sigma_o} & \text{for } \sigma \leqslant \sigma_o \\ \left(\frac{\sigma}{\sigma_o}\right)^n & \text{for } \sigma > \sigma_o;\ 1 < n \leqslant \infty \end{cases} \tag{7}$$

Here ε_o ($\equiv \sigma_o/E$) is the yield strain and n is the strain-hardening exponent. Total strain ε_t is decomposed into elastic and plastic strains ($\varepsilon_t = \varepsilon_e + \varepsilon_p$). While many indentation studies generally used Ramberg–Osgood stress–strain relation, we in the present work adopt Eq. (7), since the latter provides a distinctive linear elastic region and consequently distinctive yield strength.

3. Characteristics of indentation deformation

3.1. Deformation under indenter and characteristic of load–depth curves

We investigated the effects of friction coefficient, Young's modulus, yield strength and strain hardening exponent on load–depth curves via indentation FE analyses. Fig. 4a shows load–depth curves with variation of friction coefficient f. Here Coulomb friction coefficient f is varied from 0.1 to 0.4. Although load increases slightly with friction coefficient f for the same indentation depth, the difference is virtually negligible. While distributions of stress and strain are substantially affected by the friction coefficient, load–depth curves are almost independent of friction coefficient. In this study, a method for the evaluation of material properties is proposed with the value $f = 0.3$, and the sensitivity of the method on the friction coefficient is then discussed.

Fig. 4b shows the relations between modulus and load–depth curve. Indentation load increases for the same indentation depth as the Young's modulus increases. The effect of Young's modulus on load–depth curves is less than the other parameters but the effect cannot be ignored. It is noteworthy that unloading curves vary sensitively with Young's modulus. Fig. 4c and d shows that indentation load increases with yield strength, but decreases with strain hardening exponent for the same indentation depth. In other words, all the material properties are related to loading curves, and the slope of unloading curves is closely related to Young's modulus.

3.2. Characteristic of load–depth curves with indenter angles

Lee et al. (2008) reported that there are countless materials which have the same Kick's law coefficient C despite their different material properties. It means that stress–strain curves obtained from load–depth curves for self-similar indenters cannot be unique.

Fig. 5 shows the variations of load–displacement curves for two sets of arbitrary materials with three different half-included angles of indenter, $\alpha = 70.3°$, $60.0°$ and $45.0°$. Fig. 5a and b represents the load–depth curves for (σ_o = 800 MPa, $n = 5$; σ_o = 420 MPa, $n = 2.6$) and (σ_o = 800 MPa, $n = 5$; σ_o = 600 MPa, $n = 3.7$), respectively. Elastic moduli of them are fixed as 200 GPa. Table 1 shows that gap of C values for three indenter angles. Although there is no significant difference in C between the two materials, σ_o = 800 MPa, $n = 5$ and σ_o = 420 MPa, $n = 2.6$, for the angle of the indenter $\alpha = 70.3°$, the difference becomes about 15% for $\alpha = 45°$. In contrast to the previous case, the two materials, σ_o = 800 MPa, $n = 5$ and σ_o = 600 MPa, $n = 3.7$, show 8% deviation of C for the indenter angle $70.3°$ whereas the difference is negligible for $\alpha = 45°$. It means that two materials can be distinguished by using the two or more self-similar indenters. Note that when a lager indenter angle range is used, load–displacement curves for sets of arbitrary materials become quite separable. Based on this, we can obtain the indentation formula which converts load–depth curves to true stress–strain curves, and then suggest a dual (or plural) indentation algorithm based on FEA solutions for the material property evaluation. Table 2 shows representative material properties used in this paper, which cover the range of material property of general metals.

4. Indentation numerical approach based on finite element analysis solution

4.1. Numerical formulas for young's modulus evaluation

The slope of unloading curve, elastic recovery and contact area are related with Young's modulus (Sneddon,

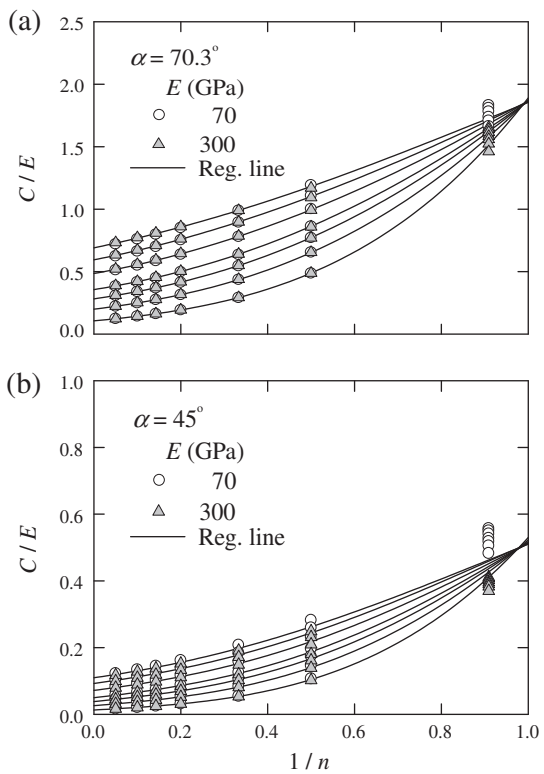

Fig. 14. Identical C vs. $1/n$ curves with ε_o for two different E (compare with Fig. 11).

1965; Taljat et al., 1997). Pharr et al. (1992) reported that the unloading curve is nonlinear, and the initial unloading slope of curve has a close relation with Young's modulus. Pharr et al. (1992) suggested the theoretical formula as follows:

$$E = \frac{1 - \nu^2}{\beta d/S - (1 - \nu_I^2)/E_I} \tag{8}$$

Here d is actual projected contact diameter considering the effect of pile-up/sink-in and S is initial unloading slope. β is the correction factor that depends on material properties and the indenter geometry. E_I, ν_I and E, ν are Young's modulus, Poisson's ratio of the indenter and the specimen respectively. Lee et al. (2008) studied the variation of β with regression range and fitting function type. For regression of unloading slope, Lee et al. (2008) considered two regression functions and two unloading ranges: power law and linear fits, and 20% and 80% of unloading data. They showed that β may be regarded as almost constant for various indentation parameters such as Young's modulus, yield strain and strain-hardening exponent and indenter tip-radius.

Table 3
Comparison of computed material properties with a WC indenter to those given.

σ_o/E σ_o (MPa)	n	Computed E (GPa)	Error (%)	Computed σ_o (MPa)	Error (%)	Computed n	Gap
0.001	2	200.3	0.1	198.3	0.9	2.0	0.00
200	3	201.3	0.6	197.2	1.4	3.0	0.01
	5	203.5	1.8	195.4	2.3	4.9	0.06
	7	203.9	2.0	197.8	1.1	7.0	0.01
	10	203.1	1.5	199.0	0.5	10.0	0.02
	13	205.2	2.6	197.0	1.5	12.7	0.27
	20	205.5	2.7	197.2	1.4	19.1	0.91
0.002	2	199.5	0.2	405.0	1.3	2.0	0.00
400	3	200.4	0.2	404.8	1.2	3.0	0.01
	5	201.7	0.8	397.3	0.7	5.0	0.04
	7	201.2	0.6	398.3	0.4	6.9	0.07
	10	203.3	1.7	398.5	0.4	10.0	0.02
	13	202.8	1.4	397.5	0.6	12.9	0.13
	20	203.6	1.8	399.0	0.3	19.9	0.14
0.003	2	199.6	0.2	598.7	0.2	2.0	0.00
600	3	199.9	0.0	591.8	1.4	3.0	0.02
	5	201.0	0.5	592.9	1.2	4.9	0.06
	7	202.3	1.2	596.8	0.5	7.0	0.00
	10	202.5	1.2	591.3	1.5	9.7	0.30
	13	202.5	1.2	593.3	1.1	12.6	0.39
	20	203.2	1.6	593.4	1.1	19.1	0.95
0.004	2	199.2	0.4	800.7	0.1	2.0	0.00
800	3	199.9	0.0	797.8	0.3	3.0	0.00
	5	200.7	0.3	794.6	0.7	5.0	0.03
	7	201.3	0.7	795.2	0.6	7.0	0.05
	10	201.5	0.8	788.0	1.5	9.7	0.30
	13	202.1	1.1	790.3	1.2	12.6	0.39
	20	203.6	1.8	787.8	1.5	18.4	1.59
0.006	2	198.2	0.9	1244.6	3.7	2.0	0.01
1200	3	200.1	0.1	1202.6	0.2	3.0	0.00
	5	200.2	0.1	1201.0	0.1	5.0	0.01
	7	199.6	0.2	1199.6	0.0	7.0	0.01
	10	200.4	0.2	1196.5	0.3	9.9	0.14
	13	200.6	0.3	1199.4	0.1	13.1	0.06
	20	200.6	0.3	1195.8	0.4	19.6	0.52
0.008	2	198.3	0.9	1634.0	2.1	2.0	0.01
1600	3	199.6	0.2	1595.0	0.3	3.0	0.01
	5	199.8	0.1	1604.7	0.3	5.0	0.03
	7	199.9	0.1	1590.8	0.6	6.9	0.11
	10	199.7	0.2	1593.3	0.4	9.8	0.17
	13	199.9	0.0	1601.3	0.1	13.1	0.11
	20	200.1	0.0	1592.7	0.5	19.2	0.82
0.010	2	198.1	0.9	2028.7	1.4	2.0	0.01
2000	3	197.8	1.1	2120.9	6.0	3.1	0.09
	5	199.5	0.3	1995.0	0.3	4.9	0.05
	7	199.1	0.4	2026.9	1.3	7.2	0.21
	10	200.0	0.0	1998.1	0.1	10.0	0.05
	13	200.1	0.0	1978.6	1.1	12.2	0.76
	20	200.0	0.0	1998.2	0.1	19.9	0.10

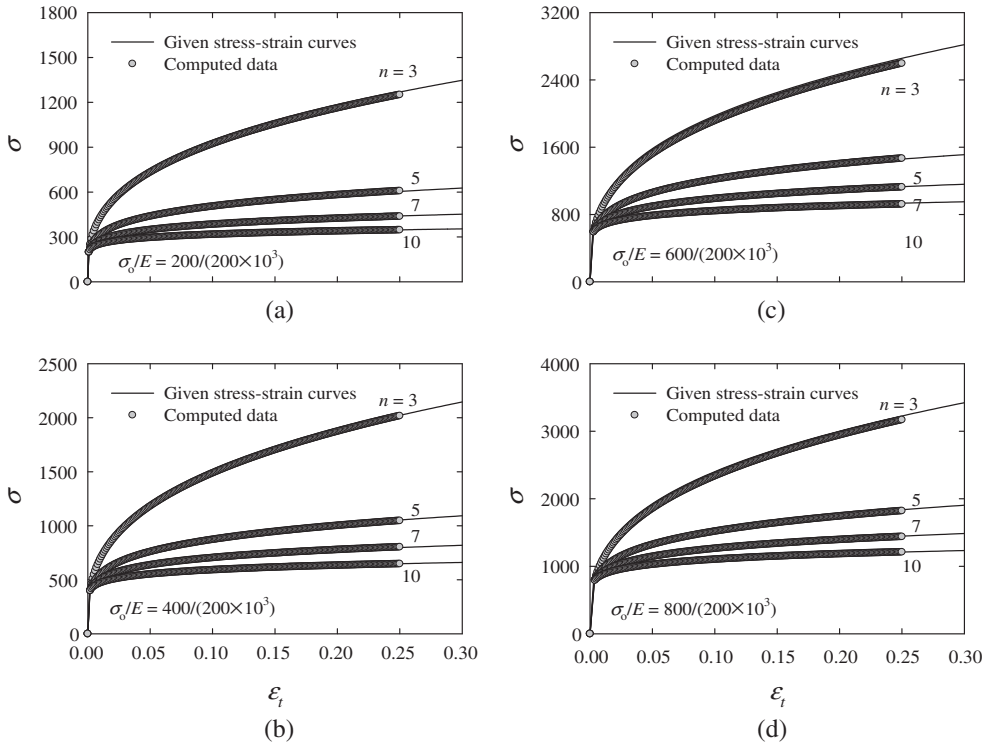

Fig. 15. Comparison of computed stress–strain curves to those given for E = 200 GPa using WC indenter [ε_o = (a) 0.001, (b) 0.002, (c) 0.003 and (d) 0.004].

When β is a constant, Lee et al. (2008) obtained four regression constants as follows:

$$\begin{aligned} \beta = 1.067; &\quad \Delta P/P_{\max} = 20\%, \text{ power law regression} \\ 1.101; &\quad \Delta P/P_{\max} = 80\%, \text{ power law regression} \\ 1.058; &\quad \Delta P/P_{\max} = 20\%, \text{ linear regression} \\ 0.987; &\quad \Delta P/P_{\max} = 80\%, \text{ linear regression} \end{aligned} \tag{9}$$

Here ΔP (=$P_{\max} - P$) is the difference between the maximum load at the maximum indentation depth and a chosen indentation load on the unloading curve (Fig. 1).

When β is a function of Young's modulus, β is given as follows:

$$\begin{aligned} &\beta = c_1 + c_2\left(\frac{E}{E_I}\right) \\ &(c_1, c_2) = (1.051, 0.04223); \quad \Delta P/P_{\max} = 20\%, \\ &\qquad \text{power law regression} \\ &\qquad (1.084, 0.04576); \quad \Delta P/P_{\max} = 80\%, \\ &\qquad \text{power law regression} \\ &\qquad (1.043, 0.04047); \quad \Delta P/P_{\max} = 20\%, \\ &\qquad \text{linear regression} \\ &\qquad (0.976, 0.02196); \quad \Delta P/P_{\max} = 80\%, \\ &\qquad \text{linear regression} \end{aligned} \tag{10}$$

Lee et al. (2008) calculated the correction factor β from Eq. (9) or (10), and obtain the Young's modulus using Eq. (8). Suggested methods successfully provide the value of elastic modulus with maximum error of less than 5%.

4.2. Calculation of contact diameter

Lee et al. (2008) calculated the Young's modulus by using Eq. (8) and projected contact diameter measured at unloading condition. In reality, it is difficult to measure the contact diameter; inaccurately obtained contact diameter can cause further error in the evaluation results. In this study, the c^2 values representing the amount of pile-up and sink-in were obtained via the FE simulation, and then the projected contact diameter was estimated. In this study, the c^2 is defined as follows:

$$c^2 \equiv (h_c|_{P_{\max}} + h_g)/(h_{max} + h_g) = f^c(\varepsilon_o, n) \tag{11}$$

Here h_c is the actual contact indentation depth considering pile-up or sink-in (Fig. 2). Fig. 6 depicts the relation between c^2 and indentation depth for four yield strains. The almost same c^2 can be obtained for various indentation depths although a considerable h_g (or tip radius R) is considered. The deviation of c^2 within the chosen $R/h_{\max}$ ratios is less than 1%. When h_g is not considered ($c^2 \equiv h_c|_{P_{\max}}/h_{\max}$), the deviation of $h_c|_{P_{\max}}/h_{\max}$ sharply increases with decreasing $R/h_{\max}$ ratio. For $h = 15h_g$, it becomes more than 4%. Fig. 7 depicts the variations of c^2 with tip-radius R ($R/h_{\max}$ = 0, 0.5, 1.0) for various material properties. Fig. 7 shows that c^2 becomes uniform for the same indentation depth regardless of tip radius, $R/h_{\max}$ = 0.5, 1.0, 2.0. Hence, indentation depth and tip-radius does not effect on value of c^2.

Fig. 8 shows the distribution of the c^2 for various material properties from obtained FE analyses. We performed

Table 4
Comparison of computed Young's moduli to those given for two different indenter angles.

σ_o/E σ_o (MPa)	n	$E_{70.3°}$		$E_{45°}$	
		Computed E (GPa)	Error (%)	Computed E (GPa)	Error (%)
0.001	3	201.3	0.6	199.3	0.4
200	5	203.5	1.8	203.2	1.6
	7	203.9	2.0	202.4	1.2
	10	203.1	1.5	202.7	1.3
0.002	3	200.4	0.2	198.7	0.6
400	5	201.7	0.8	197.5	1.2
	7	201.2	0.6	201.0	0.5
	10	203.3	1.7	203.0	1.5
0.003	3	199.9	0.0	196.2	1.9
600	5	201.0	0.5	199.1	0.5
	7	202.3	1.2	197.2	1.4
	10	202.5	1.2	200.7	0.3
0.004	3	199.9	0.0	196.7	1.6
800	5	200.7	0.3	200.5	0.3
	7	201.3	0.7	198.5	0.8

FE analyses of a total of 56 cases (yield strain ε_o: 7 × strain-hardening exponent n: 8) with fixed Young's modulus to generate regression formulae (11). The WC conical indenter with a half-included angle of 70.3° was used and the maximum indentation depth, R/h_{max}, was 0.5. In Fig. 8, c^2 value bigger than 1 means that pile-up occurs. The values of c^2 increase with strain hardening exponent and decrease with yield stain. We selected the n and ε_o as the parameters of regression function of c^2 as described in Eq. (12). In this study, the coefficients of c^2 are first regressed on n for each given ε_o, and then obtained coefficients are regressed on ε_o. Appendix A shows the regression functions and coefficients.

$$c^2 = f^c(\varepsilon_o, n) = f_i^c(\varepsilon_o)n^{-i} = (\gamma_{ij}\varepsilon_o^j)n^{-i};$$
$$i,j = 0,1,2,3,4 \quad \text{(Appendix A)} \tag{12}$$

The regression lines of c^2 for various material properties are presented in Fig. 8.

Table 5
Comparison of computed material properties with a diamond indenter to those given.

σ_o/E σ_o (MPa)	n	Computed E (GPa)	Error (%)	Computed σ_o (MPa)	Error (%)	Computed n	Gap
0.001	3	197.9	1.0	205.8	2.9	3.0	0.01
200	7	199.5	0.3	201.5	0.7	5.0	0.01
	5	199.5	0.3	201.5	0.7	7.0	0.03
	10	200.7	0.3	202.7	1.3	10.1	0.13
0.002	3	199.0	0.5	415.9	4.0	3.1	0.08
400	7	199.2	0.4	414.4	3.6	5.1	0.10
	5	201.8	0.9	413.8	3.4	7.0	0.03
	10	200.4	0.2	410.9	2.7	10.5	0.45
0.003	3	198.9	0.6	622.4	3.7	3.1	0.10
600	7	199.6	0.2	624.7	4.1	5.1	0.14
	5	199.8	0.1	623.5	3.9	7.3	0.35
	10	199.7	0.2	615.1	2.5	10.4	0.45
0.004	3	199.1	0.5	846.1	5.8	3.2	0.15
800	7	199.7	0.2	850.7	6.3	5.3	0.27
	5	199.2	0.4	846.5	5.8	7.4	0.38
	10	199.4	0.3	843.3	5.4	10.4	0.42

Table 6
Comparison of computed material properties for various R/h_{max} ratios to those given.

σ_o/E σ_o (MPa)	R/h_{max}	n	Computed σ_o/E (MPa/GPa)	Error (%)	Computed n	Gap
0.002	0.0	3	415.3/195.9	3.8/2.1	3.0	0.04
400		7	412.6/198.4	3.2/0.8	5.2	0.17
		5	412.5/196.4	3.1/1.8	7.1	0.14
		10	404.3/197.2	1.1/1.4	10.2	0.18
	0.5	3	404.8/200.4	1.2/0.2	3.0	0.01
		7	397.9/202.0	0.5/1.0	5.0	0.04
		5	401.9/201.0	0.5/0.5	7.0	0.04
		10	398.5/203.3	0.4/1.7	10.0	0.02
	1.0	3	391.5/202.8	2.1/1.4	3.0	0.04
		7	388.5/204.5	2.9/2.2	4.9	0.09
		5	389.0/205.8	2.7/2.9	6.8	0.22
		10	398.5/205.4	0.4/2.7	10.0	0.01
	1.5	3	381.7/207.4	4.6/3.7	2.9	0.06
		7	385.2/207.1	3.7/3.5	4.8	0.19
		5	388.3/206.5	2.9/3.3	6.9	0.14
		10	395.6/207.1	1.1/3.6	9.8	0.23

Knowing h_t (=h_{max} + h_g) and c^2, we can obtain projected contact diameter d by the geometrical relation of conical indenter as follows:

$$d = 2c^2 h_t \tan\alpha = 2f^c(\varepsilon_o, n)(h_{max} + h_g)\tan\alpha \quad (13)$$

Note that d becomes a function of c^2, and thereby a function of material properties ε_o and n. Using Eqs. (12) and (13), we can express Eq. (8) as

$$E = \frac{(1-\nu^2)}{2(\tan\alpha)h_t\beta f^c(\varepsilon_o, n)/S_1 - (1-\nu_I^2)/E_I} \quad (14)$$

Here S_1 is initial slope of unloading curve obtained from 70.3° indenter.

4.3. Dual conical indentation techniques for material properties evaluation

We observed the variation of coefficient C with material properties using two indenters of half-included angle 70.3°, 45° respectively. To minimize the tip radius effect, based on Lee et al. (2008)'s observation, the C values were regressed by using the data ranged upper 50% of the maximum indentation depth h_{max}.

Fig. 9 represents the distribution of coefficient C with yield strain and strain hardening exponent. In Fig. 9, the maximum value of C/E is normalized to unity. As the difference of intersection angle of contours is getting smaller, it becomes harder to distinguish the material properties although two indenters with different angle are used. As the intersection angle contoured from the two indenters is getting bigger, the properties can be more easily indentified. We calculated the gradients of contours and the angles between the gradients as shown in Fig. 10. Since strain hardening exponents of materials are generally greater than 2, it would be fair to state that most materials can be distinguished by the dual indentation tests. Noted that Chen et al. (2007) did not show clearly the applicable range of multiple indentation method, but we definitely

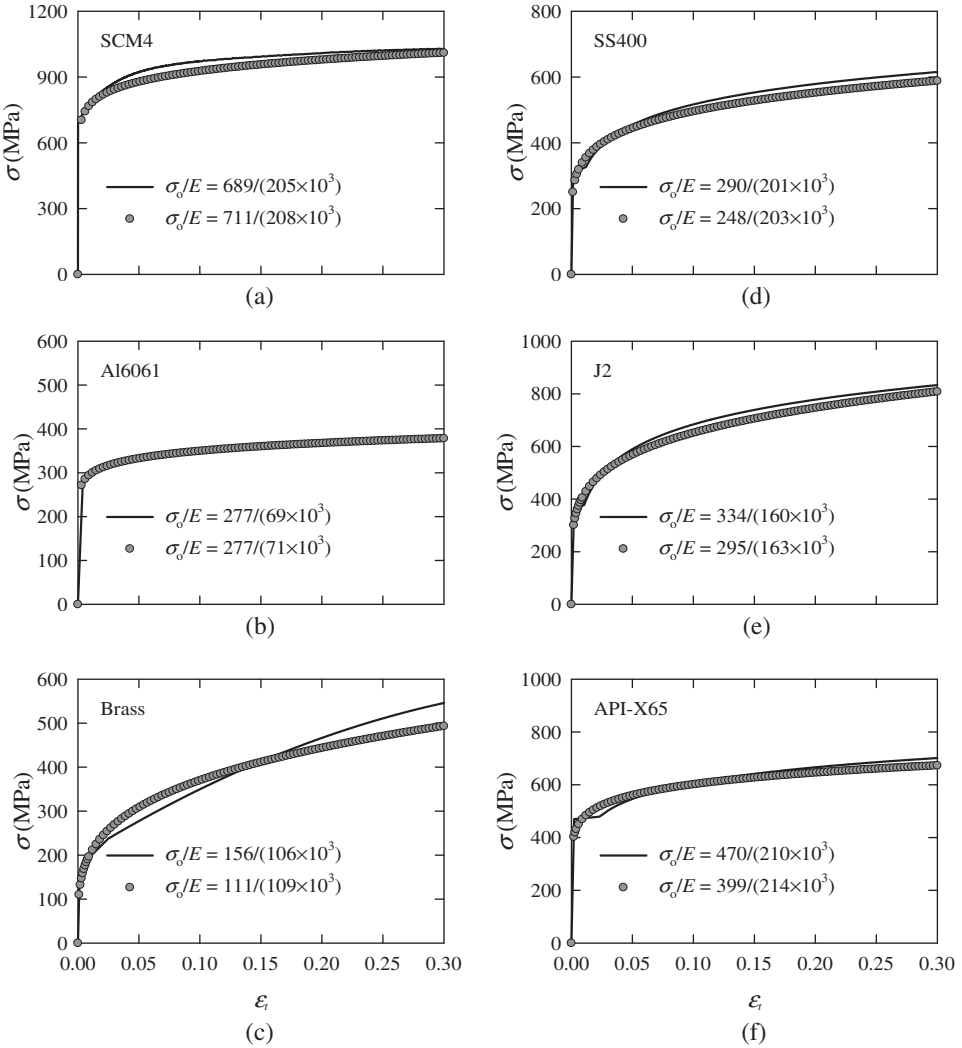

Fig. 16. Comparison of stress–strain curves computed by two parameter regression on the entire strain range to those experimentally measured for (a) SCM4, (b) Al6061, (c) Brass, (d) SS400, (e) J2 and (f) API-X65.

demonstrated the sensitivity of the predicted material properties for the two indenter angles, $\alpha = 70.3°$ and 45°.

Fig. 11a and b shows the distribution of coefficient C with yield strain ε_o, strain hardening exponent n when half-included angles of the tungsten carbide (WC) conical indenter are 70.3° and 45°; the indentation depth $R/h_{max} = 0.5$. We performed FE analyses of a total of 294 cases (Young's modulus E: 3 × yield strain ε_o: 7 × strain-hardening exponent n: 7 × half-included angle α: 2). The values of coefficient C obtained from FE analysis for various ε_o and n are regressed to dimensionless formula normalized with elastic modulus E. The regression method is the same as Eq. (12). The final regression function is a polynomial in the form of Eq. (15). The coefficients and regression curves of Eq. (15) are given in Appendix A.

$$C_i/E = f_i^C(\varepsilon_o, n) = f_{ij}^C(\varepsilon_o)n^{-j} = (\delta_{ijk}\varepsilon_o^k), n^{-j}; \quad i = 1,2; \quad j,k = 0,1,2,3,4 \quad \text{(Appendix A)} \tag{15}$$

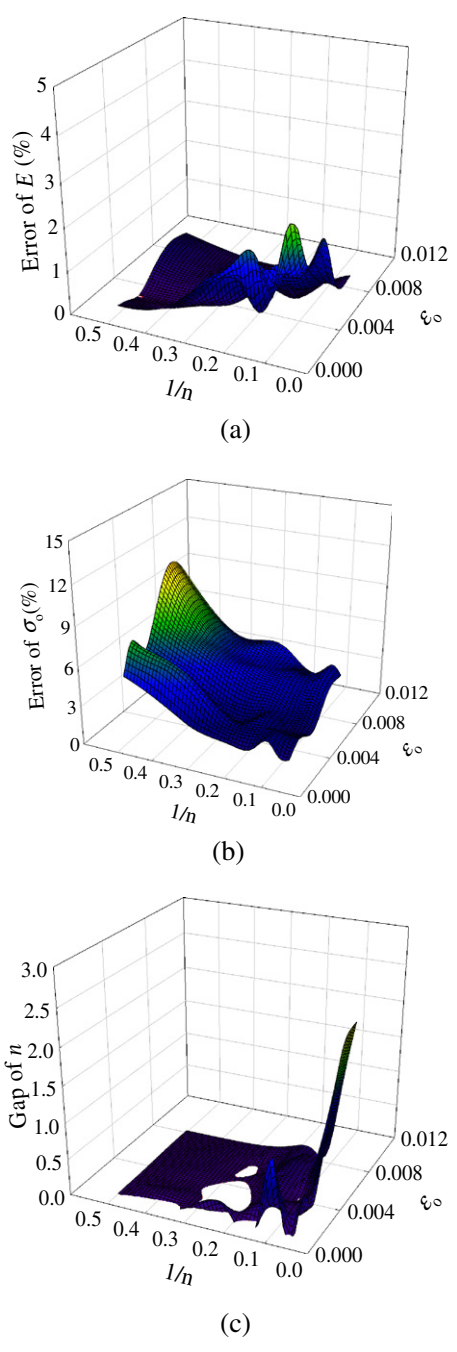

Fig. 17. Errors of computed material property values (a) E, (b) σ_o and (c) n to those given (2% increases of C_1 and C_2).

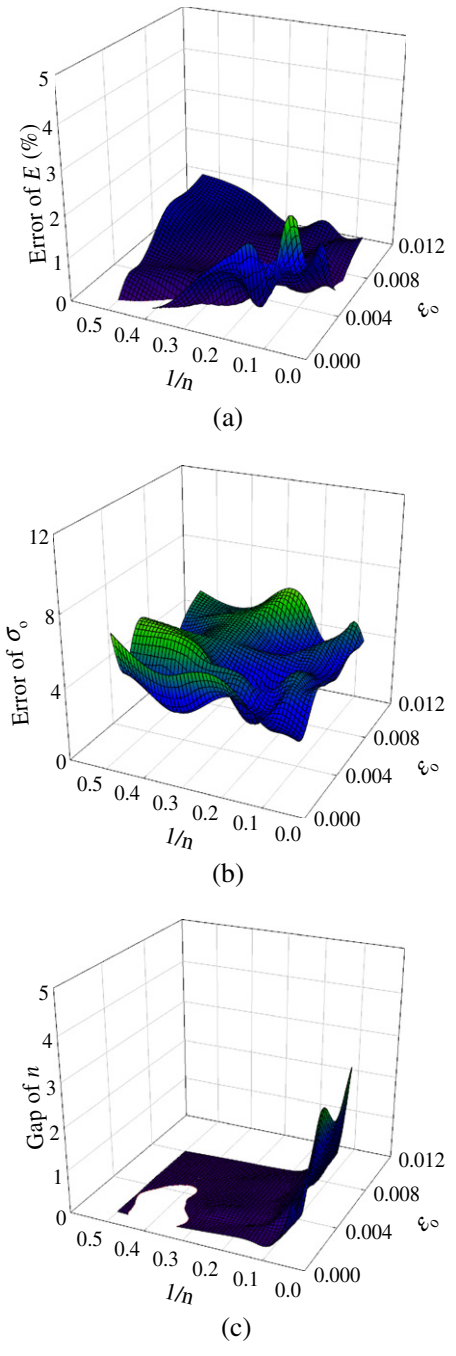

Fig. 18. Errors of computed material property values (a) E, (b) σ_o and (c) n to those given (2% decreases of C_1 and C_2).

Table 7
Sensitivity of the estimated mechanical properties to variation in the Kick's law coefficient.

Dual conical indentation						
	0% in C		+2% in $C_{1,2}$		−2% in $C_{1,2}$	
	Ave. error (%)	SD (%)	Ave. error (%)	SD (%)	Ave. error (%)	SD (%)
E	0.72	0.72	1.13	2.27	0.78	0.64
σ_o	0.94	1.02	4.80	5.60	4.50	0.94
n	1.42	1.70	3.68	7.11	3.88	3.74

Here $i = 1, 2$ represents 70.3° and 45° respectively. As C_1 and C_2 in Eq. (15) can be determined by the dual indentation tests, Eq. (15) becomes the nonlinear simultaneous equations for ε_o and n.

Substituting Eq. (14) into Eq. (15) leads to the followings:

$$
\begin{aligned}
C_1 &= E f_1^C(\varepsilon_o, n) = \frac{f_1^C(\varepsilon_o, n)}{M f^c(\varepsilon_o, n) - N};\\
F(\varepsilon_o, n) &\equiv \frac{f_1^C(\varepsilon_o, n)}{M f^c(\varepsilon_o, n) - N} - C_1 = 0\\
C_2 &= E f_2^C(\varepsilon_o, n) = \frac{f_2^C(\varepsilon_o, n)}{M f^c(\varepsilon_o, n) - N};\\
G(\varepsilon_o, n) &\equiv \frac{f_2^C(\varepsilon_o, n)}{M f^c(\varepsilon_o, n) - N} - C_2 = 0\\
M &= \frac{2(\tan\alpha) h_t \beta}{S_1(1-\nu^2)}, \quad N = \frac{(1-\nu_I^2)}{E_I(1-\nu^2)}.
\end{aligned}
\tag{16}
$$

We calculate ε_o and n which satisfy $F = 0$ and $G = 0$ of Eq. (16) using Newton–Raphson method. Based on the contact diameter at unloaded state, Lee et al. (2008) calculated $\beta = 1.058$ by linear fitting for the 20% unloading range. Meanwhile, Dao et al. (2001) used $\beta = 1.06$ in conical indentation. However, it is a very difficult that we measure the accurate contact diameter at unloading state. We can predict the actual contact diameter at unloading state, and calculate the more accurate β. In Eq. (8), we used β obtained by linear fit for 20% of unloading data. Fig. 12 shows the distribution of β obtained with linear fitting for various values of ε_o and n. The deviation of β is less than 2% irrespective of chosen material properties, β can be regarded as a constant. We adopt the mean value of $\beta = 1.068$ which is obtained in $E = 200$ GPa. Our β value is quite consistent with the other suggested material properties. Furthermore, it is very accurate for widely ε_o and n scope.

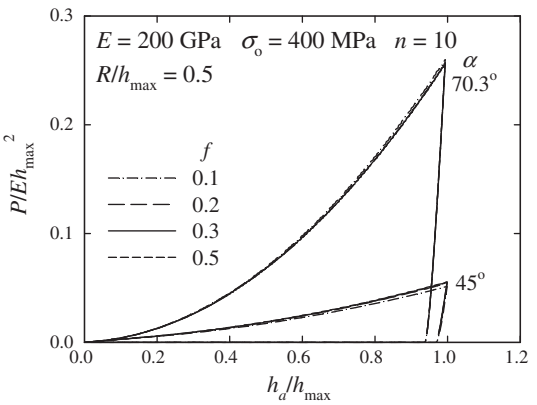

Fig. 19. $P/Eh_{\max}^2$ vs. $h/h_{\max}$ curves for four different friction coefficients.

Using Eqs. (16), we established an evaluation program providing material properties and corresponding stress–strain curve from load–displacement curves of dual conical indentation tests as shown in Fig. 13. First, we obtain the Kick's law coefficient C_1 and C_2 from load–displacement curves using two different indenters. We first set up the initial value of ε_o and n; then, we find the new ε_o and n using Eq. (16). Substituting this value for Eq. (14), we calculate the Young's modulus E. Although evaluation program providing material properties is based on $E = 200$ GPa, the program is still effective for other elastic moduli, because the relative ratio (=yield strain, ε_o) is more important indentation parameter than absolute values of elastic modulus and yield strength (Fig. 14). The obtained material properties are compared with those used for finite element analyses in Table 3. The average error of predicted material properties is less than 1%, and maximum error is about 5%. Fig. 15 shows predicted and given material curves for various material properties. The solid line is the material curve used for FEA, and the symbol is the predicted stress–strain curve. These figures show the validation of new approach for various values of n and ε_o.

In this study, we calculated the elastic modulus E by using Eq. (8). Here, the values for S and d were obtained from FE analysis using the 70.3° indenter. The projected contact diameter is a function of material properties, tip-radius and indenter angle. The contact diameter d as well as S depends on the indent angle α. If the contact diameters for various material properties using the 45° indenter are obtained from FE analyses, we can also predict the $E_{45°}$. Although the predicted values for $E_{45°}$ and $E_{70.3°}$ using Eq. (8) and (13) should be equal, their values vary slightly, although the difference is virtually negligible, due to errors

Table 8
Comparison of $P_{\max}$ values for various values of friction coefficient.

$E = 200$ GPa, $\sigma_o = 400$ MPa, $n = 10$, $R/h_{\max} = 0.5$			
α (°)	f	$P_{\max}$	Gap (%)
70.3	0.1	129.9	1.2
	0.2	128.5	0.1
	0.3	128.4	–
	0.5	128.4	0.1
45	0.1	25.7	7.6
	0.2	27.2	2.2
	0.3	27.8	–
	0.5	27.7	0.4

Table 9
Comparison of computed material property values to those given for various values of friction coefficient.

σ_o/E σ_o (MPa)	n	f	Computed σ_o/E (MPa/GPa)	Error (%)	Computed n	Gap
0.002	3	0.1	531.1/194.5	32.8/2.8	3.8	0.8
400		0.2	432.0/196.4	8.0/1.8	3.2	0.2
		0.3	404.8/200.4	1.2/0.2	3.0	0.0
	5	0.1	521.7/195.6	30.4/2.2	8.5	3.5
		0.2	428.3/198.5	7.1/0.7	5.6	0.5
		0.3	397.3/201.7	0.7/0.8	5.0	0.0
	10	0.1	506.9/195.9	26.7/2.0	62.5	2.5
		0.2	420.2/200.1	5.0/0.1	12.4	2.4
		0.3	398.5/203.3	0.4/1.7	10.0	0.0
0.004	3	0.1	993.9/193.7	24.2/3.2	3.8	0.8
800		0.2	844.1/196.4	5.5/1.8	3.2	0.2
		0.3	797.8/199.9	0.3/0.0	3.0	0.0
	5	0.1	983.0/196.4	22.9/1.8	8.2	3.2
		0.2	810.7/198.1	1.3/1.0	5.3	0.3
		0.3	794.6/200.7	0.7/0.3	5.0	0.0
	10	0.1	960.9/201.0	20.1/0.5	61.9	51.9
		0.2	795.7/201.3	0.5/0.7	10.7	0.7
		0.3	788.0/201.5	1.5/0.8	9.7	0.3
0.006	3	0.1	1429.9/193.4	19.2/3.3	3.7	0.7
1200		0.2	1252.0/196.0	4.3/2.0	3.2	0.2
		0.3	1202.6/200.1	0.2/0.1	3.0	0.0
	5	0.1	1418.7/195.3	18.2/2.4	7.9	2.9
		0.2	1199.1/197.6	0.1/1.2	5.2	0.2
		0.3	1201.0/200.2	0.1/0.1	5.0	0.0
	10	0.1	1434.5/196.9	19.5/1.5	118.4	108.4
		0.2	1181.9/198.3	1.5/0.8	10.1	0.1
		0.3	1196.5/200.4	0.3/0.2	9.9	0.1
0.008	3	0.1	1839.3/193.4	15.0/3.3	3.7	0.7
1600		0.2	1632.3/194.4	2.0/2.8	3.1	0.1
		0.3	1595.0/199.6	0.3/0.2	3.0	0.0
	5	0.1	1792.1/195.2	12.0/2.4	7.1	2.1
		0.2	1583.6/197.1	1.0/1.5	5.2	0.2
		0.3	1604.7/199.8	0.3/0.1	5.0	0.0
	10	0.1	1876.6/196.8	17.3/1.6	93.4	83.4
		0.2	1544.0/197.3	3.5/1.3	9.4	0.6
		0.3	1593.3/199.7	0.4/0.2	9.8	0.2

in the numerical calculation. However, the important thing is their accuracy. The average error of the predicted E_{45° is also less than 1% (Table 4). When we evaluate material properties using diamond indenter ($E_I = 1000$ GPa, $\nu_I = 0.07$), the obtained material properties are almost similar to those of tungsten carbide indenter ($E_I = 537$ GPa, $\nu_I = 0.24$) (Table 5). The blunted indenter tip may cause nontrivial problems in evaluating material properties. However, when tip-radii of indenters varies ($R/h_{\max} = 0$, 0.5, 1, 1.5), the average errors for ε_o and n are less than 2% and 5% (Table 6). When C is calculated, the gap h_g between indenters with zero and finite tip-radii can be determined by Eq. (2). Therefore, the finite tip-radius effect can be eliminated in the loading curve.

4.4. Evaluation of material properties by using experimentally obtained stress–strain curves

We performed the tensile and compression tests according to ASTM E8 to obtain tensile material properties. Using an MTS tensile testing system, we carried out tensile tests for round bar specimens (diameter: 6 mm) by 3 mm/min. We tested six different metallic materials: SCM4, Al6061, Brass, J2, SS400, and API-X65. We carried out the indentation test via FE analysis with the tensile testing data inputted. The stress–strain curves obtained from ten-

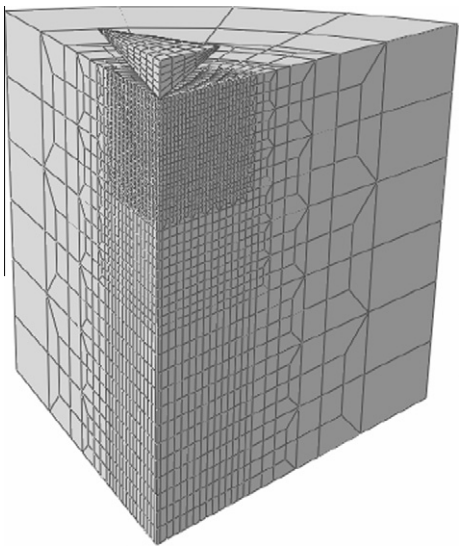

Fig. 20. Overall mesh design for 1/6 Berkovich indenter.

sile and indentation are compared in Fig. 16. Solid lines are obtained by tensile tests, the symbols are obtained by dual indentation tests. The predicted stress–strain curves almost agree well with given stress–strain curve except for Brass. The difference of yield strength between predicted (108 MP) and given (156 MPa) for Brass are large. Due to the limitation of power law expression of stress–strain curve, the difference of yield strength between predicted and given is large in the some materials not obeying power law. Moreover, a material having a large Lüders strain such as API-X65 shows a discrepancy in the early plastic region of stress–strain curve (Hyun et al., 2008).

5. Sensitivity analysis

Load–displacement curves can vary depending on the various conditions of experiment. It is therefore necessary to examine the sensitivity of evaluated material properties. Chollacoop et al. (2003), Swaddiwudhipong et al. (2005) and Harsono et al. (2009) reported that experimental scatter for Kick's law coefficient C is about 2%. We thus changed the value of C ±2% obtained from FEA with half-included angles 70.3° and 45°, and estimated the values of material properties. We confirmed the errors of predicted material properties with Kick's law coefficients for various material properties, $\varepsilon_o = 0.001$, 0.002, 0.004, 0.006, 0.008 and $n = 2$, 3, 5, 7, 10, 13, 20. Fig. 17a–c depicts the error of elastic modulus, yield strength, and the gap of strain-hardening exponent, respectively when the C_1 and C_2 are artificially increased simultaneously. On the other hand, Fig. 18a–c show the error of predicted material properties when the C_1 and C_2 are decreased simultaneously. In Figs. 17a and 18a, the maximum errors of predicted E are less than 3% regardless of variation in C. However, σ_o shows the rather strong sensitivity to variation in C than E in Figs. 17b and 18b. When we increase or decrease the values of C_1 and C_2 simultaneously, mean errors of estimated values are less than 10%. However, when C_1 is increased (or decreased) and C_2 is decreased (increased), the average of the error of the yield stress becomes about 20%. It should be mentioned that an indention system will tend to only overestimate or underestimate for the two consecutive tests because the test condition will be similar. Therefore, we can conclude that the proposed method has weak sensitivity to perturbation in input parameters, C_1, C_2. Table 7 shows the average errors and their standard deviations (SD).

Fig. 19 shows the load–depth curves for various values of friction coefficient ($f = 0.1$, 0.2, 0.3 and 0.5). Table 8 shows the gap of maximum load P_{max} with $P_{max}|_{f=0.3}$ as the base value. The load–depth curves for $f = 0.2$–0.5 are similar to that for $f = 0.3$. However, the load–depth curve for $f = 0.1$ is notably different, which may result in significant errors in material properties. We thus verify that the evaluation program established with $f = 0.3$ is valid for $f = 0.1$, 0.2. Table 9 represents predicted material properties for $f = 0.1$, 0.2 and 0.3. The errors of predicted elastic modulus are less than 4% regardless of friction coefficient.

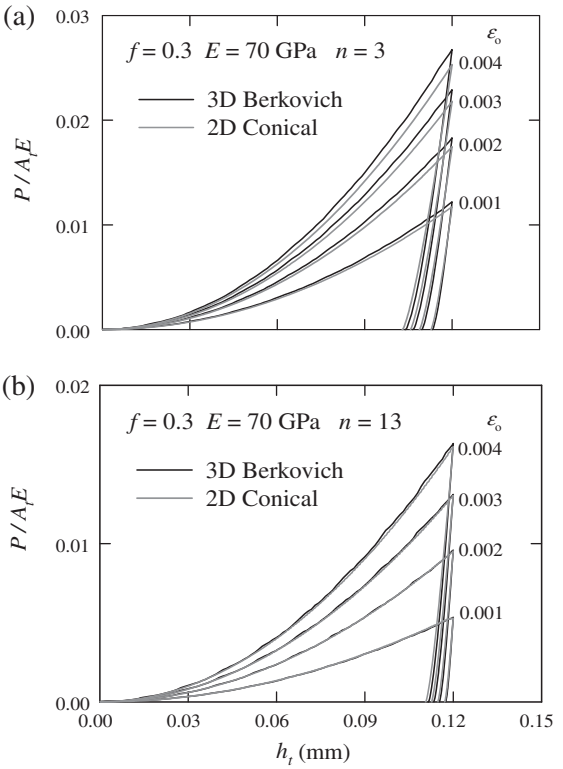

Fig. 21. Comparison of the P–h curves of conical and Berkovich indentations for four different yield strains.

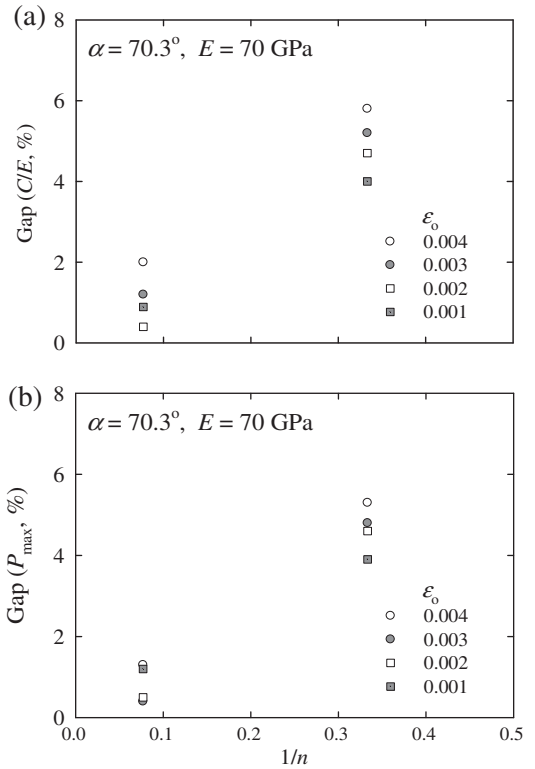

Fig. 22. Differences between conical and Berkovich indenters for (a) C/E and (b) P_{max}.

Table A.1
Values of γ_{ijk} regressed from various ε_o and n by 4th order equation.

	$k=0$	$k=1$	$k=2$	$k=3$	$k=4$
i = 1, Half-included angle α = 70.3°					
$j=0$	1.237e+0	−5.521e−1	4.756e−1	−2.850e−1	9.162e−2
$j=1$	−1.232e+0	1.028e+0	4.083e−1	−4.614e−1	−1.116e−1
$j=2$	2.458e+0	−2.798e+0	1.422e+0	−3.639e+0	2.947e+0
$j=3$	−3.914e+0	8.144e+0	−1.474e+1	2.079e+1	−1.087e+1
$j=4$	2.223e+0	−6.176e+0	1.343e+1	−1.770e+1	8.536e+0

Table A.2
Values of δ_{ijk} regressed from various ε_o and n by 4th order equation.

	$k=0$	$k=1$	$k=2$	$k=3$	$k=4$
i = 1, Half-included angle α = 70.3°					
$j=0$	2.619e−4	1.132e+0	−7.664e−1	4.523e−1	−1.277e+1
$j=1$	1.336e−1	2.179e+0	−4.100e+0	3.800e+0	−1.288e+0
$j=2$	2.535e−1	2.050e+0	−2.562e+0	2.213e+0	−1.429e+0
$j=3$	6.103e−1	3.743e+0	−1.732e+1	1.839e+1	−5.373e+0
$j=4$	9.178e−1	−9.417e+0	2.541e+1	−2.541e+1	8.362e+0
i = 2, Half-included angle α = 45°					
$j=0$	−7.811e−4	1.415e−1	−4.288e−2	1.785e−2	−5.928e−3
$j=1$	2.981e−2	4.983e−1	−6.042e−1	2.719e−1	−1.192e−2
$j=2$	−2.875e−2	5.536e−1	−1.468e+0	2.376e+0	−1.210e+0
$j=3$	2.418e−1	1.860e+0	−4.404e+0	2.865e+0	−4.754e−1
$j=4$	2.981e−1	−3.172e+0	6.703e+0	−5.658e+0	1.735e+0

For $f=0.2$, the errors in σ_o are less than 10%. For $f=0.1$, however, the maximum error in σ_o is about 30%, and the errors in n also become significant. The proposed method based on $f=0.3$ is valid for $f>0.2$, and therefore further study is required.

6. Difference between conical and Berkovich indenters

The 70.3° conical indenter theoretically has the same cross-sectional area-to-depth ratio as Berkovich indenter. Due to difference of actual contact area and contact stiffness, the load–depth curves of both Berkovich and its equivalent conical indenters are not identical (Shim et al., 2007). We compared the load–depth curves obtained from 2D conical indenter and 3D Berkovich indenter. Considering geometrical symmetry, we made the 1/6 Berkovich indenter model using the 8-node brick element C3D8 (ABAQUS, 2007). FE model consists of about 36,000 8-node brick elements (C3D8) and 45,000 nodes (Fig. 20). In an inclination surface of 60° for x axis, the ratio of displacements between x and y axis should be maintained as $1:\sqrt{3}$. The indenter downs to penetrate the material with the bottom of the specimen fixed.

When E and $R/h_{\max}$ are 70 GPa and 0, respectively, we observed the variations of the load–depth curves with strain hardening exponents ($n=3$, 13) and yield strains ($\varepsilon_o=0.001$, 0.002, 0.003, 0.004) (Fig. 21). As the n decreases and the ε_o increases, the difference between the load–depth curves obtained from conical and Berkovich indenters increases. The maximum differences of C/E and $P_{\max}$ values between conical and Berkovich are about 5% (Fig. 22). Therefore, it should be investigated the causes of the difference, and further study on the theory of Berkovich indentation is needed.

7. Summary

In this paper, we suggested the reverse algorithm for evaluation of material properties using the dual conical indentation. The proposed method successfully provides the value of material properties with the maximum error of less than 5%, regardless of tip-radius and materials properties. As mentioned in review section, while other researchers have used the concept of the representative, we provide the indentation formulae through the multi regression of material properties, σ_o/E (=ε_o) and n without the definition of representative values.

We observed the effect of conical indenter angle on indentation load–depth curves via finite element analyses. We investigated then the relations among elastic modulus, yield strength, strain hardening exponent, and load–depth curve, and we confirmed that yield strain and strain

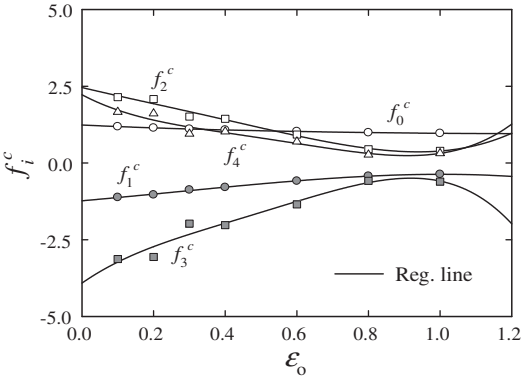

Fig. A.1. The regression curves of f^c in Eq. (11) vs. yield strain.

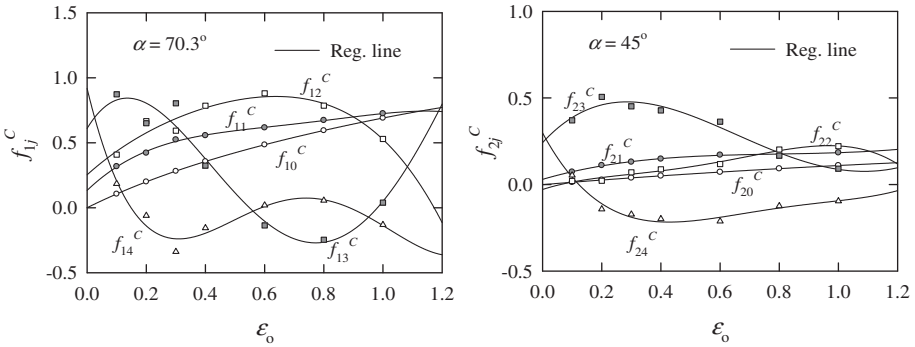

Fig. A.2. The regression curves of f_{ij}^c in Eq. (14) vs. yield strain.

hardening exponent are major parameters. We presented then the Kick's law coefficient with indenter angle as function of yield strain and strain hardening exponent. To calculate the contact diameter, we introduced the dimensionless parameter c^2, which is defined as the ratio of the tip-corrected indentation contact depth to the tip-corrected maximum depth, and then expressed it as a function of material properties. Using the c^2 and geometrical relation of conical indenter, we obtained numerical formula for evaluation of Young's modulus. Finally, we suggested an effective numerical approach for evaluation of yield strength and strain-hardening exponent using the dual conical indentation through the combination of numerical formulae. The proposed method is valid in wide range of materials properties, especially which have frictional coefficient bigger than 0.2, and the method shows weak sensitivity to perturbation of input parameters, C_1, C_2. In addition, the difference of load–depth curves obtained from a conical indenter and Berkovich indenter is discussed. Further studies on the effect of friction coefficient and the types of indenters are required.

Acknowledgments

This work was supported by the National Research Foundation of Korea (NRF) grant funded by the Korea government (MEST) (No. 2007-0052795).

Appendix A

The coefficient values of regression functions of Eqs. (11) and (14) (see Tables A.1 and A.2, Figs. A.1 and A.2).

References

ABAQUS User's Manual, 2007. Version 6.7, Hibbitt, Karlsson and Sorensen, Inc., Pawtucket, RI.

Borodich, F.M., Keer, L.M., Korach, C.S., 2003. Analytical study of fundamental nanoindentation test relations for indenter of non-ideal shapes. Nanotechnology 14, 803–808.

Borodich, F.M., Keer, L.M., 2004. Contact problems and depth-sensing nano-indentation for frictionless and frictional boundary conditions, Int. J. Solids. Struct. 41, 2479–2499.

Bucaille, J.L., Stauss, S., Felder, E., Michler, J., 2003. Determination of plastic properties of metals by instrumented indentation using different sharp indenters. Acta Mater. 51, 1663–1678.

Cao, Y.P., Lu, J., 2004. Depth-sensing instrumented indenters: stability analysis and corresponding regularization schemes. Acta Mater. 52, 1143–1153.

Capehart, T.W., Cheng, Y.-T., 2003. Determination constitutive models from conical indentation: sensitivity analysis. J. Mater. Res. 18, 827–832.

Chaudhri, M.M., 1998. Subsurface strain distribution around Vickers hardness indentations in annealed polycrystalline copper. Acta Mater. 46, 3047–3056.

Chen, W.W., Zhou, K., Keer, L.M., Wang, Q.J., 2010. Modeling elasto-plastic indentation on layered materials using the equivalent inclusion method. Int. J. Solids. Struct. 47, 2841–2854.

Chen, X., Ogasawara, N., Zhao, M., Chiba, N., 2007. On the uniqueness of measuring elastoplastic properties from indentation: the indistinguishable mystical materials. J. Mech. Phys. Solids 55, 1618–1660.

Chen, X., Yan, J., Karlsson, A.M., 2006. On the determination of residual stress and mechanical properties by indentation. Mater. Sci. Eng (A) 416, 139–149.

Cheng, Y.T., Cheng, C.M., 1998. Scaling approach to conical indentation in elasto-plastic solids with work hardening. J. Appl. Phys. 84, 1284–1291.

Chollacoop, N., Dao, M., Suresh, S., 2003. Depth-sensing instrumented indentation with dual sharp indenters. Acta Mater. 51, 3713–3729.

Cook, R.F., Pharr, G.M., 1990. Direct observation and analysis of indentation cracking in glasses and ceramics. J. Am. Ceram. Soc. 73, 787–817.

Dao, M., Chollacoop, N., Vliet, J.V., Venkatesh, T.A., Suresh, S., 2001. Computational modeling of the forward and reverse problems in instrumented sharp indentation. Acta Mater. 49, 3899–3918.

Giannakopoulos, A.E., Larsson, P.-L., 1997. Analysis of pyramid indentation of pressure-sensitive hard metals and ceramics. Mech. Mater. 25, 1–35.

Giannakopoulos, A.E., Suresh, S., 1999. Determination of elastoplastic properties by instrumented sharp indentation. Scripta Mater. 40, 1191–1198.

Harsono, E., Swaddiwudhipong, S., Liu, Z.S., 2009. Materials characterization based on simulated spherical-Berkovich indentation test. Scripta Mater. 60, 972–975.

Huber, N., Tsakmakis, C., 1999a. Determination of constitutive properties from spherical indentation data using neural networks. Part I: the case of pure kinematic hardening in plasticity laws. J. Mech. Phys. Solids 47, 1569–1588.

Huber, N., Tsakmakis, C., 1999b. Determination of constitutive properties from spherical indentation data using neural networks. Part II: plasticity with nonlinear isotropic and kinematic hardening. J. Mech. Phys. Solids 47, 1589–1607.

Hyun, H.C., Lee, J.H., Lee, H., 2008. Mathematical expressions for stress–strain curve of metallic material. Trans. KSME 32, 21–28.

Kermouche, G., Loubet, J.L., Bergheau, J.M., 2008. Extraction of stress–strain curves of elastic–viscoplastic solids using conical/pyramidal indentation testing with application to polymers. Mech. Mater. 40, 271–283.

Lan, H., Venkatesh, T.A., 2007. Determination of the elastic and plastic properties of materials through instrumented indentation with reduced sensitivity. Acta Mater. 55, 2025–2041.

Le, M., 2008. A computed study on the instrumented sharp indentations with dual indenters. Int. J. Solids. Struct. 45, 2818–2835.
Le, M., 2009. Materials characterization by dual indenter. Int. J. Solids. Struct. 46, 2988–2998.
Lee, H., Lee, J.H., Pharr, G.M., 2005. A numerical approach to spherical indentation techniques for material property evaluation. J. Mech. Phys. Solids 53, 2037–2069.
Lee, J.H., Kim, T., Lee, H., 2010. A study on robust indentation techniques to evaluate elastic–plastic properties of metals. Int. J. Solids. Struct. 47, 647–664.
Lee, J.H., Lee, H., Kim, D.H., 2008. A numerical approach to elastic modulus evaluation using conical indenter with finite tip radius. J. Mater. Res. 23, 2528–2537.
Liao, Y., Zhou, Y., Huang, Y., Jiang, L., 2009. Measuring elastic–plastic properties of thin films on elastic–plastic substrates by sharp indentation. Mech. Mater. 41, 308–318.
Ogasawara, N., Chiba, N., Chen, X., 2005. Representative strain of indentation analysis. J. Mater. Res. 20, 2225–2234.
Ogasawara, N., Chiba, N., Chen, X., 2006a. Limited analysis-based approach to determine the material plastic properties with conical indentation. J. Mater. Res. 21, 947–957.
Ogasawara, N., Chiba, N., Chen, X., 2006b. Measuring the plastic properties of bulk materials by single indentation Test. Scripta Mater. 54, 65–70.
Ogasawara, N., Chiba, N., Chen, X., 2009. A simple framework of spherical indentation for measuring elastoplastic properties. Mech. Mater. 41, 1025–1033.
Oliver, W.C., Pharr, G.M., 1992. An improved technique for determining hardness and elastic modulus using load and displacement sensing indentation experiments. J. Mater. Res. 7, 1564–1583.
Pharr, G.M., Oliver, W.C., Brotzen, F.R., 1992. On the generality of the relationship among contact stiffness, contact area and elastic modulus during indentation. J. Mater. Res. 7, 613–617.
Rice, J.R., Rosengren, G.F., 1968. Plane strain deformation near a crack-tip in a power law hardening material. J. Mech. Phys. Solids 16, 1–12.
Shim, S., Jang, J., Pharr, G.M., 2008. Extraction of flow properties of single-crystal silicon carbide by nanoindentation and finite-element simulation. Acta Mater. 56, 3824–3832.
Shim, S., Oliver, W.C., Pharr, G.M., 2007. A comparison of 3D finite element simulation for Berkovich and conical indentation of fused silica. Int. J. Surf. Sci. Eng. 1, 259–273.
Sneddon, I.N., 1965. The relation between load and penetration in the axisymmetric Boussinesq problem for a punch of arbitrary profile. Int. J. Eng. Sci. 3, 47–57.
Suresh, S., Giannakopoulos, A.E., 1998. A new method for estimating residual stresses by instrumented sharp indentation. Acta Mater. 46, 5755–5767.
Swaddiwudhipong, S., Tho, K.K., Liu, Z.S., Zeng, K., 2005. Material characterization based on dual indenters. Int. J. Solids. Struct. 42, 69–83.
Tabor, D., 1951. The Hardness of Metals. Oxford University Press.
Taljat, B., Zacharia, T., Kosel, F., 1997. New analytical procedure to determine stress–strain curve from spherical indentation data. Int. J. Solids. Struct. 35, 4411–4426.
Tho, K.K., Swaddiwudhipong, S., Liu, Z.S., Zeng, K., Hua, J., 2004. Uniqueness of reverse analysis from conical indentation test. J. Mater. Res. 19, 2498–2502.
Xia, S.M., Gao, Y.F., Bower, A.F., Lev, L.C., Cheng, Y.-T., 2007. Delamination mechanism maps for a strong elastic coating on an elastic–plastic substrate subjected to contact loading. Int. J. Solids 44, 3685–3699.